atmosphere

MDPI

Article

An Assessment of the Weather Research and Forecasting Model for Solar Irradiance Forecasting under the Influence of Cold Fronts in a Desert in Northwestern Mexico

Jose Ernesto López-Velázquez [1,*], Nicolás Velázquez-Limón [2,*], Saúl Islas-Pereda [2], David Enrique Flores-Jiménez [1], Néstor Santillan-Soto [1] and Juan Ríos-Arriola [2]

[1] Laboratorio de Ciencias Atmosféricas Aplicadas, Instituto de Ingeniería, Universidad Autónoma de Baja California, Mexicali 21280, Mexico; david.flores80@uabc.edu.mx (D.E.F.-J.); nsantillan@uabc.edu.mx (N.S.-S.)
[2] Centro de Estudios de las Energías Renovables, Instituto de Ingeniería, Universidad Autónoma de Baja California, Mexicali 21280, Mexico; islass@uabc.edu.mx (S.I.-P.); riosj9@uabc.edu.mx (J.R.-A.)
* Correspondence: ernesto.lopez16@uabc.edu.mx (J.E.L.-V.); nicolas.velazquez@uabc.edu.mx (N.V.-L.); Tel.: +52-686-551-82-22 (J.E.L.-V.)

Abstract: Northwestern Mexico has a desert climate with high solar resources. Clear skies and low humidity during most of the year favor their use. In winter, the arrival of cold air masses from the polar latitudes cause instability and abrupt changes in atmospheric variables, increasing the error of short-term forecasts. This work focuses on the evaluation of the Weather Research and Forecasting (WRF) model for predicting the global horizontal irradiance (GHI), considering different parameterizations of shortwave and longwave solar radiation during the influence of five cold fronts that affected the desert region of northwestern Mexico. The simulation was carried out under four main shortwave configurations and the results were evaluated with surface measurements and compared with climate information from NASA-POWER. The GHI predicted with the Dudhia parameterization showed an overestimation of the WRF model during most of the analyzed events; the most accurate predictions obtained correlation values between 0.85 and 0.91 and a mean absolute error between 15 and 45 W m^{-2}. In periods where intermittent clouds prevailed, the mean error increased by almost 20%. An evaluation of the different proposed configurations shows advantages with the shortwave Dudhia and longwave RRTM parameterizations, providing a useful meteorological tool for predicting short-range variations in the GHI to improve the operability of solar power generation systems.

Keywords: desert climate; WRF; cold fronts; global horizontal irradiation; operational forecast; solar radiation variability

Citation: López-Velázquez, J.E.; Velázquez-Limón, N.; Islas-Pereda, S.; Flores-Jiménez, D.E.; Santillan-Soto, N.; Ríos-Arriola, J. An Assessment of the Weather Research and Forecasting Model for Solar Irradiance Forecasting under the Influence of Cold Fronts in a Desert in Northwestern Mexico. *Atmosphere* **2024**, *15*, 1300. https://doi.org/10.3390/atmos15111300

Academic Editor: Eugene Rozanov

Received: 23 August 2024
Revised: 27 September 2024
Accepted: 4 October 2024
Published: 29 October 2024

1. Introduction

Solar power plants are a promising solution to reduce greenhouse gas emissions into the atmosphere. Some studies have shown that the influence of cloudiness, ambient temperature, and humidity are closely related to the accurate prediction of solar irradiance variability, which directly affects power generation (e.g., Refs. [1–4]). Concentrated solar power (CSP) uses direct solar irradiation to heat fluid until it vaporizes, then introduces the vapor into an expander to generate mechanical work, which in turn drives an electrical generator; photovoltaic (PV) technologies harness global solar irradiance and convert it into electrical energy from semiconductor materials. In both cases, the prediction of solar irradiance is crucial for the operability of power grids, allowing for better planning and regulation of variable power generation [5]. In the residential, commercial, agricultural, and industrial sectors, it is expected that solar-activated power generation systems (SGESs) will gradually become accessible and affordable technologies for any user; they will continue their large-scale expansion in various climatic regions, and will see sustained research and development in the coming years. Therefore, the prediction of solar power generation will become increasingly necessary in the short range [6,7].

However, one of the greatest vulnerabilities of SGESs lies in the uncertainty of the intermittency and natural variability the resource can generate, especially during mesoscale meteorological events and extreme events; in the United States alone, it has been reported that between 2000 and 2021, approximately 83% of interruptions in the electric grid were attributed to extreme meteorological events, which annually affect the safety and public health of citizens, in addition to causing damage to the electric infrastructure. Severe weather events such as high winds and storms (58%), winter weather events (22%), and tropical cyclones (15%) were among the top causes of power outages. Texas, Michigan, and California stood out as the states with the most weather-related power outages [8].

For example, in 2010, a cold snap in France caused a spike in natural gas demand, with approximately every degree Celsius drop in temperature resulting in an increase of 100 GWh in daily natural gas consumption. In January 2017, Spain experienced a three-day period with a minimum temperature of 1.8 °C, which, combined with winter weather conditions, market restrictions, and the need to supply electricity to France due to the failure of its nuclear power plants, drove prices up to EUR 112.8 per MWh, the highest ever recorded in the Spanish region [9].

The need for adequate weather forecasting to increase the reliability of electricity generation in power plants supplied by renewable resources has become relevant in North America. In February 2021 in Texas, USA, the slow movement of an intense cold front associated with an Arctic air mass caused several events that interrupted the electricity supply to almost 10 million people for several days. During the influence of the weather system, the generation of the main energy sources in Texas (natural gas, wind, coal, nuclear, and solar) decreased, which, in a cascading effect resulting from the extreme winter conditions, led to a significant deficit in the generation of natural gas, causing an over-demand of the available energy; as well as the death of 111 people due to the impact of the winter system [10].

In the western United States, southern California, Arizona, and part of the desert area of northwestern Mexico between Baja California and Sonora, there is a region of extreme desert climate that is of particular interest for study due to its interaction with extreme weather events in winter; according to the Climate and Weather Disaster Report for California and Arizona from 1980 to 2024, severe storms, freezes, and floods during the winter season can cause significant stress on energy demand in the region [11].

Over the southwestern United States and northwestern Mexico, winter frontal systems occur between September and May, with an average of 55 events per season, according to historical weather reports from the National Meteorological Service of Mexico (SMN) over the past 10 years. Considering the historical data on the occurrence of winter frontal systems based on the synoptic analysis of the Weather Prediction Center [12] archives, approximately 40% of the total frontal systems each season enter the western and southwestern United States, affecting Southern California and Baja California.

Weather forecasting considers two important time scales to differentiate the variability that affects the prediction of the solar resource: (1) Medium-range forecasts, which are mainly influenced by long-term weather patterns in the atmosphere that may include periods longer than 120 h or correspond to climatic oscillations that regulate the meteorological conditions of a region for long periods as annual cycles or longer [13]. The second scale of interest, which is the focus of this analysis, involves a smaller temporal and spatial coverage and is known as (2) short-range forecasting. This scale includes variations related to meteorological phenomena lasting from a few minutes to about 72 h and with spatial coverage ranging from 0.01 km to 100 km. Some meteorological phenomena, such as storms, tornadoes, and cold fronts, produce variations in solar irradiance that develop within the spatial and temporal horizons that can be predicted by short-range weather forecast [14], as shown in Figure 1.

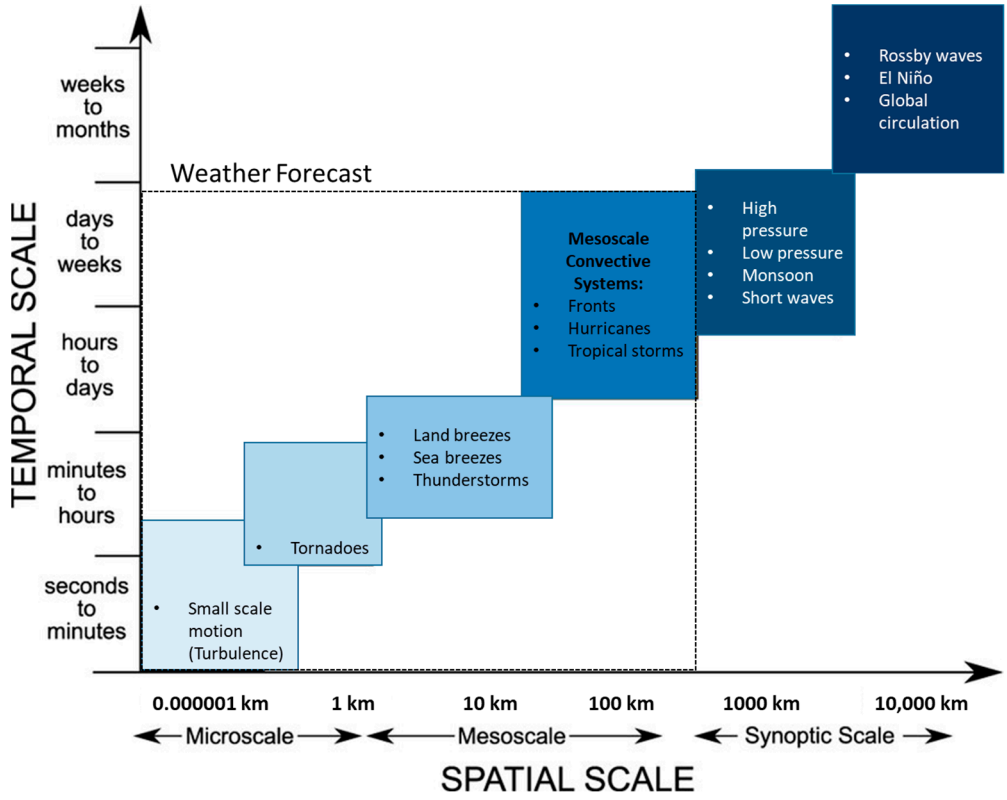

Figure 1. Time scales of weather and climate prediction with reference to the spatial and temporal horizons of some atmospheric phenomena (modified from [15]).

Climate models are a fundamental tool in the investigation of long-range atmospheric variations; they are capable of representing general patterns of temperature, humidity, and precipitation over a large region; however, their low resolution makes it difficult to analyze spatial scales smaller than 100 km. Among the forecasting methods capable of capturing local variability are statistical models (SMs) and numerical weather prediction (NWP) computational models. Statistical models require a robust climate and meteorological database of the site, from which meaningful statistical relationships are established for the prediction of atmospheric variables [16]. NWP can be based on initial data available from different global models, satellite data, and reanalysis information. They also allow for the configuration of high-resolution domains for a specific region and offer the possibility of selecting different physical parameterizations of atmospheric processes for small-scale experimental purposes. Among the studies that have focused their interest on the short-range prediction of solar irradiance at sites with potential for solar energy harvesting, we can mention [17], whose authors conducted an evaluation of the Weather Research and Forecasting (WRF) model in the region of Andalusia, Spain, using three-day periods throughout 2007 and 2008 to collect clear, partially covered and cloudy days in different seasons of the year. The results of the model showed that there was a greater number of successes in the prediction of solar irradiance during spring and summer, while fall and winter showed greater inaccuracies. Cohen et al. [18] conducted a review of planetary boundary layer (PBL) parameterization schemes, such as Yonsei University (YSU), Quasi-Normal Scale Elimination (QNSE), Mellor–Yamada–Janjic (MYJ), Asymmetric Convective Model 2 (ACM2), and Medium-Range Forecast Model (MRF), by simulating a cold season in the southeastern United States (winter–spring), where the simulation of humidity and temperature meteorological variables under severe convective weather conditions was analyzed. The results showed the advantages and disadvantages of local and non-local parameterizations during the influence of mesoscale systems, where the implementation of the YSU parameterization in the PBL was particularly notable. In a similar effort to

evaluate parameterization schemes, in 2016, the authors of [4] conducted a study over a large region of Greece, characterized by a Mediterranean climate. This study involved the simulation and analysis of one year of horizontal solar irradiance measurements, focusing on the variation in shortwave parameterization schemes in the WRF model for clear day cases and "all cases", which included different cloudiness conditions. The statistical results showed that clear days were satisfactorily predicted under the Dudhia parameterizations, but in the rest of the cases, different parameterizations stood out according to the seasons of the year. In 2019, Ref. [5] evaluated different WRF model parameterizations for global solar irradiance prediction in a Mediterranean climate in the southeastern region of Turkey. The study simulated different periods of the year to characterize the model's behavior in different seasons. Among its results, the study highlighted the favorable performance of the shortwave FLG and RRTMG parameterizations, and it retained YSU as its only variation in the PBL parameterizations.

In 2020, the authors of [19] performed a short-range forecast in Australia with the WRF-Solar model, with an emphasis on the simulation of solar irradiance and meteorological variables for 24–48 h periods, which they called "high solar intermittency days"; these were selected over a year of on-site measurements based on the determination of the clearness index, which partially related the interaction with the influencing cloudiness. Among their most outstanding results, the authors pointed out that the prediction errors in wind speed and direction were closely related to the cloudiness circulation. These results gave rise to works such as the one carried out by the authors of [20], in which, under the continuation of the search for improvements for short-range solar prediction and the influence of other meteorological variables related to the interaction with cloudiness, they selected several periods of temperate climate for the northeastern region in Germany, which were considered relevant to their variability on that time scale. They simulated periods in which the region was influenced by cold, warm, and occluded frontal systems. The RRTMG and Dudhia schemes were used, and it was found that the most favorable prediction results were obtained with RRTMG for almost all cases, except for occluded fronts.

Based on the background information, which shows that no studies have been conducted to predict solar irradiance in desert climates during winter seasons, this paper presents an evaluation of the WRF model for the prediction of the global horizontal irradiance (GHI) by simulating five cold fronts over the desert region of northwestern Mexico, recorded between 2017 and 2020. The events were selected for having registered abrupt changes in GHI, ambient temperature (Tamb), and relative humidity (Hrel), in addition to having a similar duration and having generated clouds at different times of the day.

Each experiment was run under four different configurations of solar radiation settings of the WRF model. The results obtained were compared with surface measurements from automatic weather stations, solar pyranometers, satellite data, and a reference to a persistence forecast. The Dudhia and RRTMG parameterizations of the WRF allow for a more accurate estimation of the behavior of the GHI variable during the passage of the cold fronts, which can be used to make a better short-term prediction of the electricity generation of the solar power plants in the event of short-range meteorological events, as well as allowing for the planning and definition of operational strategies in solar power plants.

2. Materials and Methods

In order to predict the variability of solar irradiance during the influence of winter frontal systems in the desert region of northwestern Mexico, the following steps were carried out: an analysis of the synoptic behavior of mesoscale systems, a selection of the case study sample (winter cold fronts), configuration of the WRF computational model, definition of domains, and selection of the solar radiation parameterizations. Finally, the results were statistically evaluated to analyze the performance of each proposed configuration and to identify which conditions showed the best results for evaluated frontal systems. The methodology used is shown in detail below.

2.1. Geographical and Climatological Description of the Study Area

The area of focus for this study is the desert zone of northwestern Mexico, with the city of Mexicali, Baja California, selected as a representative point, given its exposure to the extreme events characteristic of this region. The city of Mexicali is situated on the border with the United States, in the extreme northwest of Mexico (N 32°30′18.468″, W −115°8′51.756″). It is bordered to the north by the US state of California and to the northeast by the US states of Arizona and Sonora. During the summer months, the average maximum temperature is 42 °C, with occasional readings reaching 45 °C. In contrast, the average minimum temperature during the winter months (December to February) is 9 °C, with occasional readings reaching 2.5 °C [21]. During the summer months, the maximum GHI reaches 1200 W m^{-2}, with 600 W m^{-2} recorded on some winter days. One of the primary meteorological phenomena affecting the northwestern desert region during the winter season is the occurrence of cold fronts, which span from September to May, with the majority occurring between December and March. As [22] notes, frontogenesis occurs when two air masses, one cold and the other warm, collide. The cold air mass displaces the warm air mass, and the surface separating both is called a "cold front". A cold front (CF) generates significant vertical displacement within the atmosphere. The air forced to rise is cooled adiabatically, resulting in the formation of low and medium clouds, as well as large convective clouds. These clouds are associated with storms, fog, or heavy rain, and they can occur in a relatively short period of time. Additionally, maximum temperatures decrease and wind speeds increase as a result of cold fronts. As illustrated in Figure 2, the CF events documented in the study region have their origin in the vicinity of the North Pole. They commonly traverse a portion of the west coast of the United States and reach northern Mexico, where they may either move southward within the country or eastward across the southeastern border region. They may also traverse the northern and central regions of the United States before reaching Mexican territory or approach lower latitudes to the east, ultimately entering the Gulf of Mexico. A synoptic situation of particular interest for this study can also occur, in which a CF with characteristics of a maritime polar (mP) or tropical maritime (mT) air mass moves over the west coast of the United States, acquires a greater influence of Pacific Ocean moisture, and enters northwestern Mexico (Figure 2). The duration of these mesoscale systems in northwestern Mexico can vary from one to four days, similar to that described by the authors of [23] in their study of the passage of cold fronts over the northwestern coasts of the Gulf of Mexico. They are typically associated with moderate rainfall, a decrease in maximum temperatures, and an increase in wind speeds. Their influence can also result in the formation of partial clouds, which contributes to a significant short-range variability of the GHI.

To meet the duration and variability criteria for a typical winter event in the study region, Table 1 presents a selection of five cold fronts that affected the northwestern area of Mexico between 2017 and 2020. These events were identified using data from the Mexicali, Baja California meteorological station and NASA data base viewer [24]. As this study classifies frontal systems according to the characteristics of the cold air masses associated with them, including polar maritime (mP), tropical maritime (mT), and polar continental (cP) air masses, it was essential to observe the displacement of each frontal system in historical synoptic maps at least 48 h prior to its arrival in the study region. This classification allows for the association of an additional descriptive characteristic in relation to each event.

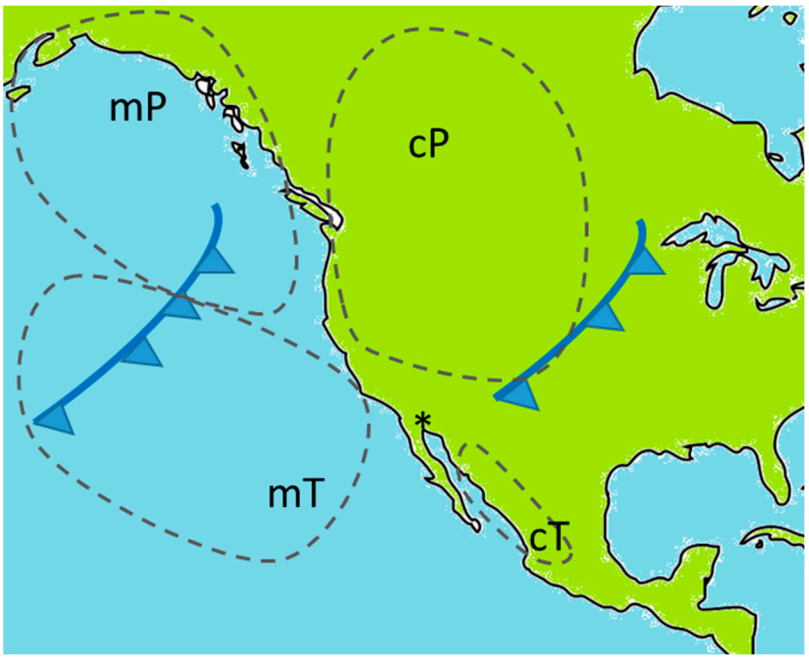

Figure 2. Graphical representation of the air masses associated with winter frontal systems affecting northwestern Mexico, depending on their origin: maritime tropical (mT), maritime polar (mP), continental polar (cP) and continental tropical (cT). Own elaboration. The symbol "*" indicates the location of Mexicali, Baja California (own reproduction).

Table 1. Events (cold fronts) simulated in the experiments.

Event	Air Mass-Associated	Year	Date
CF01	Maritime polar (humid)	2017	January 17 to 21
CF02	Maritime polar and tropical (humid)	2017	February 15 to 19
CF03	Maritime polar (humid)	2018	January 18 to 22
CF04	Continental polar (dry)	2018	December 20 to 24
CF05	Maritime polar and tropical + post Tropical storm influence (humid)	2020	November 5 to 9

2.2. Measured Data

The initial conditions of the WRF model are based on the Final Operational Global Analysis (FNL) data from the National Center for Prediction and the Environment (NCEP). This dataset has a spatial resolution of 1° × 1° and a temporal resolution of 6 h, 26 vertical levels, and global coverage [25]. To validate the results obtained with the WRF model, they were statistically compared using data measured by an automatic weather stations model Davis Vantage Pro2 and a pyranometer model CMP-10 (Kipp & Zonen, Delft, The Netherlands), installed at the UABC Engineering Institute, Mexicali, Baja California, as representative of the study region (Figure 2). To verify the accuracy of the simulation results, corresponding hourly data were also collected from the NASA-POWER climate database, which is a satellite/reanalysis model [24] and has been used in some studies to estimate weather variables and test their reliability against meteorological measurements [26,27]. Additionally, the results were compared with data from the persistence forecast, which is a term used in weather forecasting to indicate that there is no change in the weather from one day to the next. As noted by [28], forecasters frequently identify instances where a forecast model exhibits suboptimal performance and hypothesize the presence of a persistent error in the model when similar conditions occur again. To this end, it is essential to quantify the discrepancy of a suboptimal forecast model across successive days, regardless of the

prevailing meteorological conditions. This enables forecasters to assess the potential for model enhancement and identify the critical areas of divergence within the simulation [29].

2.3. Model Setup and Parameterizations

WRF is a numerical weather prediction (NWP) model and an atmospheric simulation system designed for research and operational applications [30]. It represents the state of the atmosphere in a three-dimensional grid in terms of fundamental variables and is considered a non-hydrostatic model that solves the primitive equations that describe the atmospheric circulation. It also allows for forecasting meteorological variables with a high resolution from initial and boundary conditions. Within the model, there is the possibility of configuring parameters that influence physical atmospheric processes related to radiation, convection, and cloud microphysics, among others. These processes take place mainly at low levels of the atmosphere and are represented by modules called physical parameterizations, which consist of algorithms that calculate the effect of the phenomenon indirectly from the variables that the model is able to resolve, and once resolved, the effect or trend is applied to underlying fields of the domain proposed for a study area in the model [31].

The main variations that affect solar radiation during its passage through the atmosphere are mostly due to cloud scattering processes; however, aerosol scattering and humidity also play an important role. Many NWP models have minimized the effects of aerosol scattering, and have limited themselves to the use of climate data to substitute for the lack of measurement methods to obtain these values in the modeled area. This simplification has led models to make errors of up to 20% in their predictions [32].

More and more models include advanced shortwave (SW) solar radiation parameterizations based on two-stream or four-stream solvers of the radiative transfer equation (RTE) in multiple spectral bands [33]. The RRTMG [34] and its predecessor RRTM schemes [35], used in this research, are examples of schemes that combine the need for global and regional models in solar prediction. The RRTMG scheme focuses on the representation of variations due to water vapor, carbon dioxide, nitrogen, aerosols, Rayleigh scattering, and cloudiness; this scheme and RRTM have great similarity, but their major difference lies in their multiple scattering calculations and subscale parameterizations of cloudiness.

Under clear sky conditions, RRTMG can be expected to have a prediction error of about 0.3% with respect to RRTM [34]. The Goddard scheme, used in this research, was developed by NASA at the Goddard Space Flight Center for application to climate models [36]. Goddard is similar to the Fu-Liou-Gu (FLG) scheme, also implemented in the modeling proposed in this research, since it calculates the radiative flux from the 4- and 2-stream delta methods for 6 spectral bands, less than any other previous scheme [37]. The WRF model has more than 10 schemes in SW and longwave (LW) radiation. The four parameterization schemes mentioned for SW (RRTMG, RRTM, FLG, and Goddard) partially correspond to the methodology used by [5] for Turkey, where it was implemented under different cloud cover conditions with the purpose of identifying the best model configuration that favored the GHI prediction, as they implement different algorithms for radiative flux calculations, the representation of different numbers of spectral bands, and the simulation of different scattering sources such as gases and aerosols. Some similar configurations of SW solar parameterizations for WRF also stood out for their exploration in previous studies and their validity in the model (e.g., Refs. [4,19,20]).

2.4. Domains and Configuration

Three domains were used, a parent domain (D01) and two nested or interior domains (D02 and D03), as detailed in Figure 3. In these domains, a 3:1 resolution ratio was maintained, with the highest resolution in D03 having a grid spacing of 2.3 km, centered at the point of surface measurements. The domains were sized in this way in order to capture the occurrence and progressive displacement of the CF developing offshore to the northwest and entering from the west of the region.

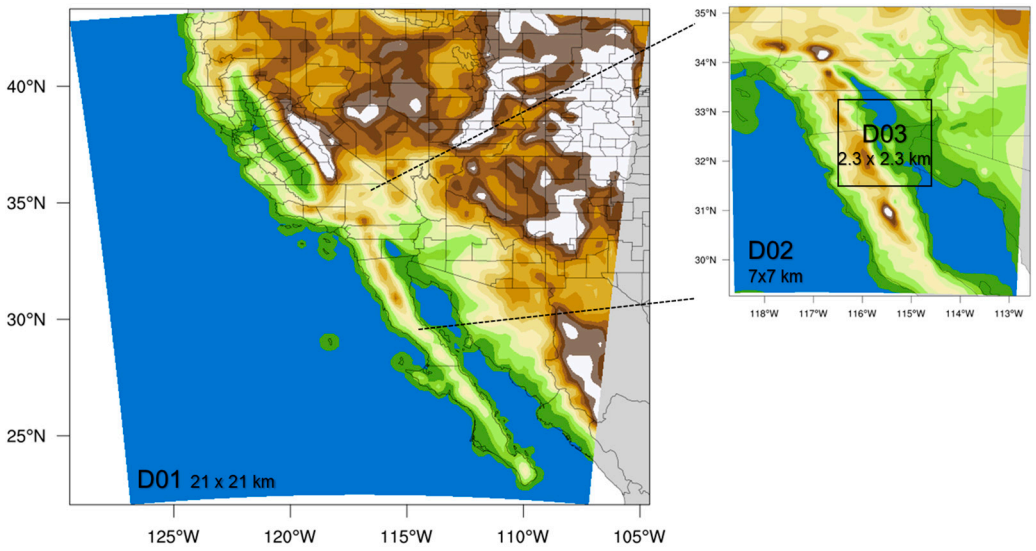

Figure 3. Domains of the simulations of the study area. D01 and D02 consider the southwestern United States, northern Mexico, and part of the Pacific Ocean and the Gulf of California; and D03 contains the representative area of Mexicali, Baja California (own preparation).

All experiments comprised a simulation period of 120 h (Table 1). The simulations were performed with the WRF-Solar model version 4.3 [30] and four different configurations were applied, as shown in Table 2. The focus of this work on improving the GHI prediction proposed mainly varied the radiation parameterizations in four combinations of SW and LW, while the rest of the parameters such as microphysics, surface, and cumulus only underwent necessary changes due to the compatibility of the options with each other. In the parameterization of the planetary boundary layer (PBL), YSU was used, based on the results that showed the experimentation performed for a winter–spring season in the southeastern United States by [18]. The results of all simulations were extracted from the highest resolution domain (D03), according to the coordinates of the meteorological station from which the measurements were obtained.

Table 2. Configurations used in the simulation of each event.

Parameterization	**Option 0**	**Option 1**	**Option 2**	**Option 3**
Radiation SW/LW	RRTMG / RRTM	FLG / FLG	Dudhia / RRTM	N Goddard / N Goddard
Microphysics	WSM6	Thompson	WSM6	Goddard ICE
Surface Layer	Monin Obukhov	Monin Obukhov	Monin Obukhov	Monin Obukhov
Surface Physics	Noah	Noah	Noah	Noah
Cumulus	Kain Firtsch	Kain Firtsch	Kain Firtsch	Kain Firtsch
PBL	YSU	YSU	YSU	YSU

2.5. Statistical Metrics

For the evaluation of the results, the statistical errors between the simulated data in D03 (Figure 3) and the measured data of GHI, ambient temperature (Tamb), and relative humidity (Hrel) were calculated with a total number of data N= 720 for each event. The mean absolute error (MAE) represents the measure of the closeness between the measured and simulated values in terms of absolute value (1). The mean bias (MBIAS) is represented in units of the variable measure of the mean trend of the simulated and measured values, where values close to zero are the most favorable, positive values indicate an overestimate, and negative values an underestimate (2). The root-mean-squared error (RMSE) was also

calculated, which gives more weight to the mean dispersion of the errors individually (3) [38].

A Taylor diagram compares modeled and observed values, and several of which are used to show a statistical summary of how the results of a model's output agree in terms of dispersion and correlation with each other; standard deviation is shown in the x- and y-axes and Pearson's correlation coefficient is pointed out at the circumference of the diagram [39]. The normalized reference values for GHI, Tamb, and Hrel correspond to the measured values and are located at the bottom center of the figure.

$$MAE = \sum_{i=1}^{N} \frac{|Xmeasured - Xforecasted|}{N} \quad (1)$$

$$MBIAS = \frac{1}{N}\left(\sum_{i=1}^{N}(Xmeasured - Xforecasted)\right) \quad (2)$$

$$RMSE = \sqrt{\frac{1}{N}\sum_{i=1}^{N}(Xmeasured - Xforecasted)}^{2} \quad (3)$$

3. Analysis and Discussion of Results

This paper presents the forecast results of the GHI in a WRF model for cold frontal systems in a desert region. In order to perform the simulation of the selected events, four different configurations of physical parameterizations were tested, opt0, opt1, opt2, and opt3, which were proposed for the prediction of short-term irradiance variability due to the influence of other meteorological variables and cloud circulation by mesoscale events, as mentioned previously in Table 2. Given the extent of the statistical comparison performed for the five frontal events and the similarity of the results obtained for events CF01, CF02, CF03, and CF04, only the prediction errors of the most favorable case (CF01) and the least favorable case (CF05) are discussed and compared. Furthermore, the analysis of these two cases is of great interest in the evaluation of the WRF model due to the contrasting characteristics under which the frontal systems were classified: the first (CF01), as a "wet" event, is mainly associated with a polar maritime air mass, and the second (CF05) is mainly associated with a tropical maritime air mass and the influence of synoptic conditions particular to the transition season from autumn to winter in the study region, as mentioned above in Table 1.

3.1. Variability of Cold Fronts in a Case Study

In order to analyze the correlation and variability of the forecast with respect to the observed data, the forecasted data series of frontal systems CF01 and CF05 were plotted by variables in scatter plots. They were differentiated into diurnal (10:00 am to 5:30 pm) and nocturnal (6:00 p.m. to 9:30 a.m.) periods as shown in Figures 4 and 5. In Figure 4, corresponding to CF01, it is possible to observe that the GHI showed a behavior with a marked linear trend and the greatest dispersion of points graphed was observed from values above 500 W m^{-2} for most of the options, i.e., a large number of the predictions commit a similar estimation error. Within the GHI, it can be highlighted that some data points corresponding to opt1 are located further apart from the data cloud than the rest, mainly in overestimates in the range of 400–700 W m^{-2}. With a similar behavior, in the range of 300–700 W m^{-2}, the points corresponding to opt3 showed overestimates. The scatter plot for the GHI shows coherent results for the predicted values in the night period, ranging from 0 to 30 W m^{-2}. Tamb groups most of its values within a linear trend and shows a greater scatter of points at values above 12.5 °C. The lower temperature values, in the range of 7.5 to 11 °C, show a good correlation with respect to the measured values, and the night periods predominate. Temperatures between 11 and 20 °C show that the points are dispersed to the left of the data cloud as an underestimation of the day and night data of opt2, and to the right, in the same range as a diurnal, an overestimation of opt0

and opt3. In the Hrel variable, it is observed that the lowest dispersion of points is located between the values in the range of 20 and 40%, mainly in diurnal periods; while the rest of the values show a gradual increase in dispersion as they approach values greater than 60%. In the Hrel values, the daytime and nighttime periods are homogeneously dispersed in the 40–60% range, showing an overestimation, and this behavior is highlighted in the axis of the predicted values upon observing the dispersion of points in the 60–80% range for opt2; in the same range, but in the axis of the measured values, most of the options in daytime and nighttime periods are an underestimation.

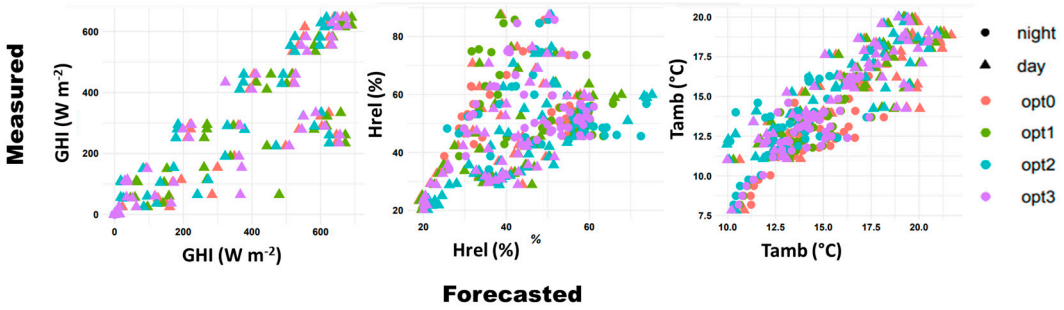

Figure 4. Scattering points differentiated in night and day periods of the solar radiation, relative humidity, and ambient temperature variables (**left** to **right**) with respect to the data predicted in the CF01 event.

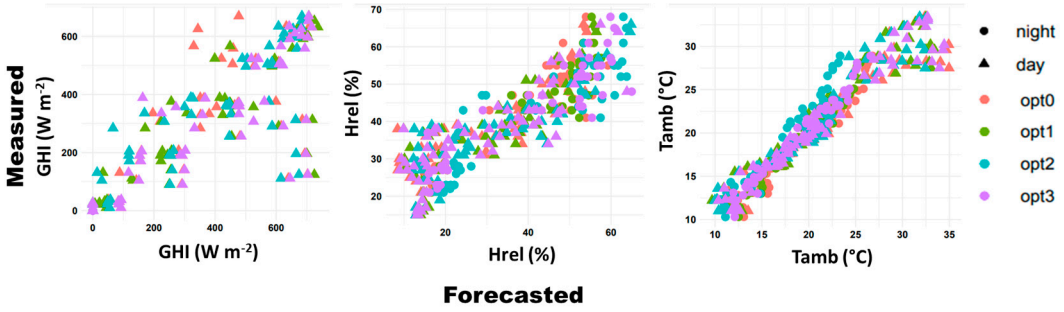

Figure 5. Scattering points differentiated in night and day periods, of the solar radiation, relative humidity, and ambient temperature variables (**left** to **right**) with respect to the data predicted in the CF05 event.

Figure 5, corresponding to event CF05, shows that the GHI is the variable with the greatest dispersion in the point cloud and that the estimates show a greater dispersion within the range of 400–700 W m^{-2}. It is possible to distinguish its positive linear trend; however, the errors that the prediction makes by overestimating or underestimating values equal to or greater than 600 W m^{-2} in most of the options stand out. With regard to the overestimates, opt2 and opt3 stand out, while for the underestimates, it is opt0. The Tamb is generally grouped with a clear positive trend and little dispersion of points in the data. The highest values in the range of 30–35 °C in diurnal periods, which show possible overestimates at values above 30 °C, stand out for their greater dispersion. The Hrel also shows a dispersion of data that tends to a linear correlation. The data cloud is more dispersed in the area of the minima and maxima values of the series, although underestimates predominate. However, although the differentiation between daytime and nighttime data is not clear, since they are homogeneously distributed in the data cloud, a normal pattern of behavior can be observed by locating a majority of nighttime points in the region of maximum values (greater than 50%), and of daytime periods in the region of the graph with the minimum values (below 30%). Both the overestimates shown by the GHI and Tamb could be due to the variability generated by the meteorological event upon arrival at the study point, which generated a significant error in the model's prediction

due to the abrupt change in these variables by influencing the humid air mass, which is reflected in the diurnal underestimates. The overestimation of the Hrel conditions of CF01 was what marked the main difference with respect to CF05, in addition to favoring a greater variability of Tamb of the former with respect to the latter. The conditions of underestimation of the GHI for CF05 were not present in CF01 in a significant way.

3.2. Taylor Diagrams

The results obtained with the different proposed configurations were also compared graphically in terms of Pearson's correlation coefficient values and standard deviation, normalized with a Taylor diagram as shown in Figures 6 and 7. In Figure 6, corresponding to event CF01, it is observed that the variable with the highest similarity to the observed data was the GHI in the data measured by NASA, with correlation values around 0.98, followed very closely by the opt2 configuration prediction in the same variable. The rest of the forecast options for the GHI variable were very close to each other with values around a Pearson's correlation of between 0.92 and 0.94 and a standard deviation close to 1. The persistence forecast representing the variability with respect to the previous day, as expected due to the influence of the frontal event, was the least favorable prediction, with correlation values close to 0.82. The predictions of the Tamb variable showed Pearson's correlation values between 0.85 and 0.89 in the proposed configuration options (opt0, opt1, opt2, and opt3), which were grouped with similar values and a standard deviation close to 1. The values measured by NASA in Tamb obtained one of the lowest correlation values with 0.82 and a standard deviation of approximately 1.50, which could be due to the differences in resolution in the mesh of the model. The persistence forecast showed correlation values of 0.88, similar to the prediction options, which showed that there was no significant ambient temperature variability during the frontal event. The Hrel predictions in CF01 presented the least favorable correlation values compared to the rest of the normalized variables, as well as a higher standard deviation with values close to 2. The correlation values in Hrel were less than 0.60 in all the proposed options; opt0, opt2, and opt3 showed very similar values between them, ranging between correlations of 0.40 and 0.55. Given the characteristics of CF01, favorable values were obtained in the prediction of solar irradiance, followed by the Tamb variable, with the least favorable prediction being Hrel.

From Figure 7, corresponding to the Taylor diagram of event CF05, it is possible to observe that one of the best-predicted variables was Tamb, with correlation values that ranged from 0.85 to 0.97. The Hrel and GHI variables showed similarity, with most of their predictions ranging from 0.75 to 0.9 and standard deviations between 1.5 and 2; however, opt1 in both variables can be considered as the most favorable results for Hrel and GHI, followed closely by opt2 with similar values. In this same comparison, the data measured by NASA were favorable in the prediction of the GHI and Tamb, but not so for Hrel, where, despite showing a correlation higher than 0.9, a standard deviation close to 2 was obtained. This is possibly associated with local conditions of moisture transport at low levels of the atmosphere, which NASA measurements failed to represent. As mentioned above, it is important to note that in event CF05, the GHI predictions were less favorable than in CF01, i.e., the local humidity factor at the study site during the passage of the frontal system generated errors in the model predictions. The results of the GHI predictions in the two frontal events showed that the proposed prediction options were more favorable in the CF01 event, which is associated with a polar maritime air mass; in the prediction of event CF05, the standard deviation values were higher, possibly due to the influence of the tropical maritime air mass with the influence of ODALYS, a weak and short-lived tropical storm that remained over the western portion of the Eastern Pacific basin from 3 to 8 November with a peak on 4 November and low remnants from 5 to 8 November [40].

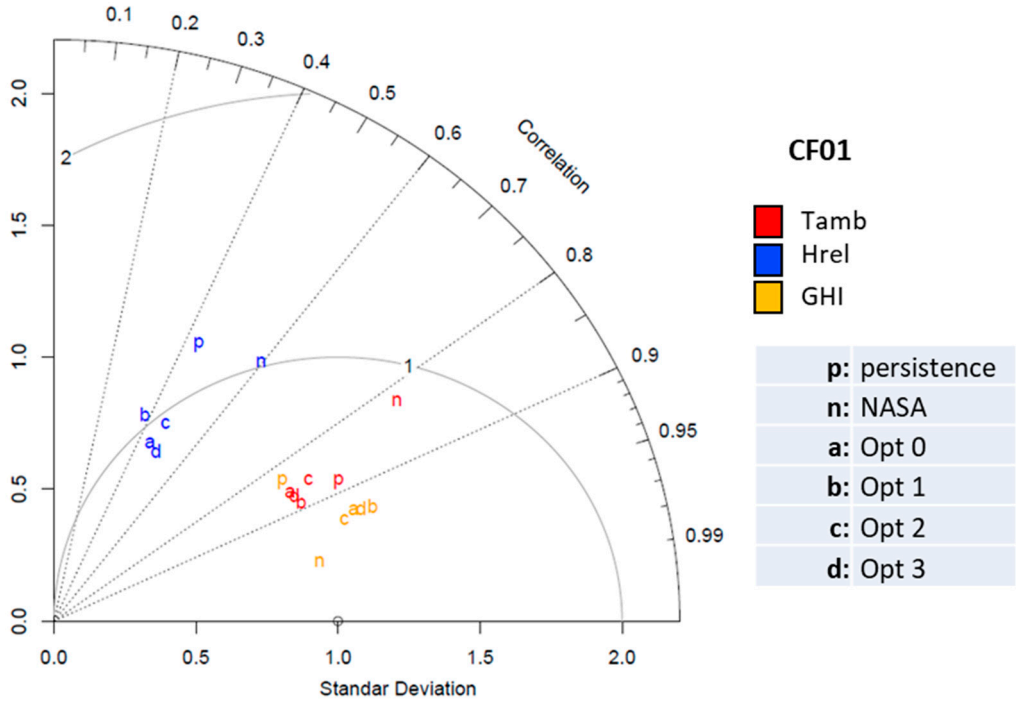

Figure 6. Taylor diagram of the results of the GHI (yellow), Tamb (red), and Hrel (blue) for the CF01 event.

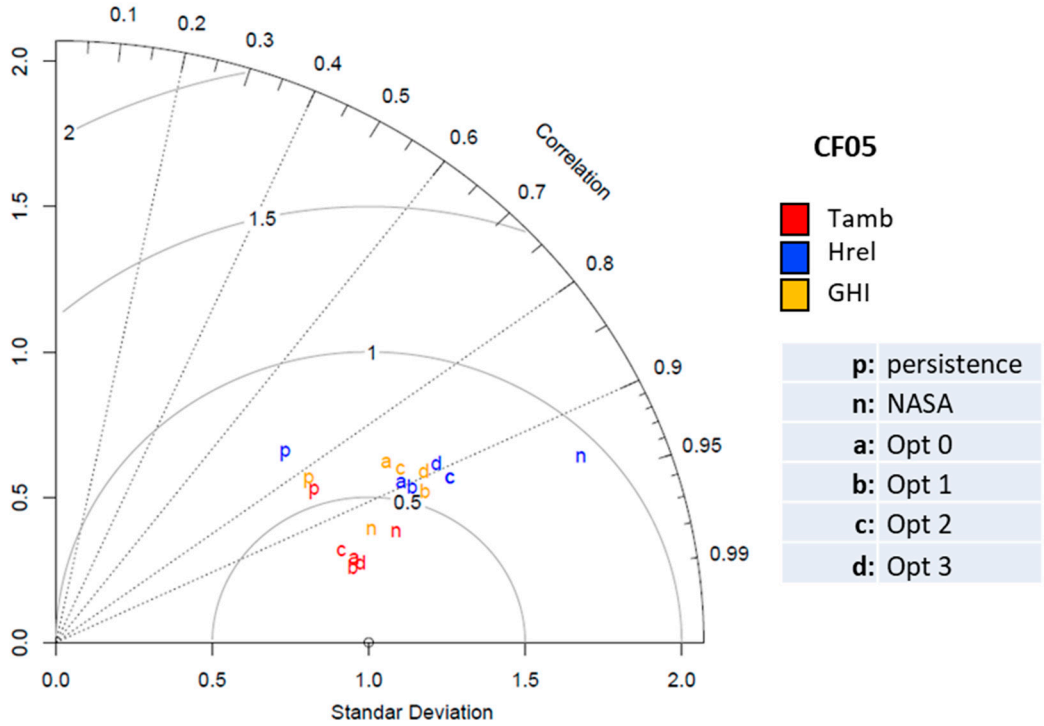

Figure 7. Taylor diagram of the results of the GHI (yellow), Tamb (red), and Hrel (blue) for event CF05.

3.3. Analysis of Statistical Values

Table 3 shows the statistical values of the CF01 forecast classified as a system with greater influence of a polar maritime air mass. Considering the characteristics of each statistic used to quantify the error in the simulations, it is necessary to analyze and discuss every result for each of the variables. In the statistical results, it is observed that opt2 predominates over the rest of the configurations for most of the simulated variables.

Table 3. Results of R^2, MAE, MBIAS, and RMSE for the prediction results for each configuration option for event CF01.

CF01	opt0	opt1	opt2	opt3	NASA	Persistence	
GHI	0.86	0.86	0.87	0.86	0.94	0.69	R^2
Tamb	0.74	0.78	0.73	0.75	0.67	0.78	
Hrel	0.2	0.143	0.21	0.23	0.35	0.19	
GHI W m^{-2}	41.15	40.65	35.66	42.13	22.4	53.12	MAE
Tamb °C	1.7	1.36	1.23	1.32	2.42	1.19	
Hrel %	13.12	13.11	12.26	12.44	14.3	14.57	
GHI W m^{-2}	−29.1	−39.21	−16.2	−28.6	−2.96	4.96	MBIAS
Tamb °C	−1.43	−1.04	−0.22	−0.88	1.72	0.1	
Hrel %	10.57	9.45	5.27	9.54	−8.96	−0.34	
GHI W m^{-2}	92.3	101.5	81.36	95.06	48.5	116.7	RMSE
Tamb °C	2.05	1.7	1.56	1.68	2.99	1.51	
Hrel %	17.96	18.53	15.75	16.92	18	17.77	

For the GHI variable, the determination coefficient R^2 shows values between 0.69 and 0.94. The values measured by NASA obtained the most favorable estimate with an R^2 of 0.94; however, there was no significant difference between the proposed prediction options, which ranged between 0.86 and 0.87. The persistence forecast showed the lowest coefficient value with an R^2 of 0.69, suggesting an attribution to the daily variability generated by the event. A similar pattern of correlation was observed in the statistical results for the Tamb and Hrel variables, where the R^2 of the simulation options showed values between 0.73 and 0.78, and 0.14 and 0.23, respectively. The R^2 values for the Hrel variable were the least favorable of the proposed configuration options.

In the MAE statistic, the GHI simulation option corresponding to opt2 was considered the best result because its values were the lowest among the options with 35.66 W m^{-2} and with an error 18% lower than the rest; in the measured data from NASA, the lowest value was obtained with 22.35 W m^{-2}, which represents a difference of only 35% with respect to the opt2 simulation. For the Tamb and Hrel variables, the MAE values in the opt2 configuration options were also the most favorable with a difference of approximately 40% in Tamb and 9% in Hrel with respect to the rest of the options.

For the GHI variable, all the proposed simulation configurations showed a negative MBIAS: opt2 with a value of −16.22 W m^{-2}, while the rest had higher negative values up to −39 W m^{-2}, in contrast to opt1. The RMSE statistic showed a similar pattern for opt2, where, with a value of 81.36 W m^{-2}, it was the best evaluated configuration option. The MBIAS values were the most favorable across the board, i.e., the lowest values of this statistic for the GHI were from NASA were from NASA and the persistence forecasts with a value of −2.96 and 4.96 W m^{-2}, respectively; however, with only a difference of −13.2 W m^{-2}, opt2 was the best of the predictions. Of the proposed configuration options, opt2 showed the most favorable values for most of the statistics, except for R^2, where the predictions were evaluated with values that were similar to each other with only a difference of one-tenth.

The variables Tamb and Hrel obtained a favorable estimation with low values in most of the statistics. Tamb showed R^2 values between 0.67 and 0.78, with the highest value in opt1, similar to that of the persistence forecast and slightly different from opt2 with 0.73, which dominated in the rest of the statistics. Finally, it is important to note that the measured NASA data, for the R^2, MAE, MBIAS, and RMSE statistics in Tamb and Hrel, made errors that, at times, in the statistical evaluation, resulted in scores that were a less favorable "prediction" than some of the proposed options.

The statistical results of the CF05 event, classified as wet and with the influence of a tropical cyclone prior to its displacement in the study area, are shown in Table 4. The GHI variable showed the most favorable values of R^2 in the opt1 with 0.86, while the opt0

was the least favorable, with 0.77 followed by the persistence forecast with a value of 0.68. In MAE, a similar pattern to the previous event could be observed, since according to the values, the best evaluated option was opt1 with 47.14 W m^{-2}, followed only by opt2 with 47.55 W m^{-2}; the MBIAS values remained negative in all options, where opt2 showed a lower bias with −22.81 W m^{-2}, in contrast to the highest bias, corresponding to opt3, with −43.95. W m^{-2}. The RMSE reflected that the values of 104.35 W m^{-2} and 108.33 W m^{-2} for opt1 and opt2, respectively, were the most favorable and did not show a large difference between them. As can be seen in the CF05 statistics, it is not possible to appreciate a clear trend towards any of the proposed options; however, relevant values were identified in almost all the options except opt0.

Table 4. Results of R^2, MAE, MBIAS, and RMSE for the prediction results for each configuration option for event CF05.

CF05	opt0	opt1	opt2	opt3	NASA	Persistence	
GHI	0.77	0.86	0.82	0.83	0.94	0.68	R^2
Tamb	0.93	0.93	0.91	0.94	0.89	0.67	
Hrel	0.78	0.79	0.79	0.78	0.84	0.42	
GHI W m^{-2}	55.98	47.14	47.55	55.51	20.94	51.63	MAE
Tamb °C	1.14	1.16	1.52	1.08	2.13	3.38	
Hrel %	7.92	7.37	6.91	7.67	9.7	9.27	
GHI W m^{-2}	−29.62	−34.53	−22.81	−43.95	−5.95	−2.09	MBIAS
Tamb °C	−0.4	0.06	0.91	0.18	0.98	−2.45	
Hrel %	6.72	6.17	3.7	5.05	−1.53	3.53	
GHI W m^{-2}	120.58	104.35	108.33	119.63	49.07	126.61	RMSE
Tamb °C	1.66	1.57	2.01	1.53	2.67	4.39	
Hrel %	9.83	9.54	9.12	9.7	11.84	11.34	

The Tamb and Hrel variables showed a satisfactory estimation in most of the statistics for each of the configuration options. However, according to the small differences shown in the evaluation, it could be complicated to define an optimal option. The Tamb variable showed good results, especially in opt3, where R^2, MAE, and RMSE were the most favorable among the configuration options. For the Hrel variable, it can be highlighted that there are unfavorable statistical values compared to the rest of the variables; this was generally the least accurate prediction in the CF05 event; however, opt2 stood out as the configuration with the best statistical results. Its highest R^2 value was obtained in opt1 and opt2 with 0.79.

4. Conclusions

In this work, four proposed configurations of the WRF model's physical parameterizations are generated and evaluated, focused on the prediction of the GHI for five frontal systems in the study region. The Tamb and Hrel are of great variability during this type of winter events, so they were considered in the discussion of the predicted GHI behavior. Based on the dispersion analysis of the point series, the evaluation of statistical errors between measured and calculated values, and their respective correlations, it can be concluded that the predictions of the GHI, Tamb, and Hrel variables within a range no larger than two standard deviations were able to simulate the behavior of atmospheric conditions during the passage of a winter frontal system. However, according to the evaluation of the statistical results obtained in all the case studies, the opt2 configuration corresponding to the Dudhia and RRTM solar radiation parameterizations was the most favorable for most of the events.

During the period of influence of the frontal systems analyzed in the study region, it was perceived that the WRF model made errors of underestimation and showed a lack of sensitivity to the rapid variability generated by possible clouds and humidity at low levels of the atmosphere, which was visible during the first 12 h, in which the cold front

entered the study region. For the most part, it is clear that opt2 dominated with the most favorable statistical prediction values. Predictions of the Tamb variable obtained the lowest errors despite a general overestimation evidenced in the MBIAS values. The predictions of Hrel showed different values in the errors; however, they did not exceed the MAE of 13% nor the 10.6% overestimation in the less favorable cases. The fact that the Hrel variable responded with low correlation values and a relatively high error percentage could be closely related to the behavior and natural variability of the on-site measurements. Given the characteristics of the CF05 study event, this analysis suggests that the WRF model has difficulty in predicting the variability of the humidity of a cold front associated with a tropical maritime air mass and its interaction with Pacific upwelling moisture associated with the passage of tropical cyclones that transport moist air masses from latitudes to the south.

The results of the data measured by NASA stood out as a potential tool for the adjustment of the case studies analyzed, mainly due to the low errors shown in their measurements when recording the Hrel and GHI variables during the influence of frontal events associated with humid air masses.

The comparison between the persistence forecast and the predictions generated by the four WRF model parameterization configurations showed the capacity of the model to improve the prediction of atmospheric variables under the influence of cold fronts. Based on the observation of the Taylor diagrams and the analysis of the statistical errors, it can be concluded that the model configuration corresponding to the opt2 had the best performance in the prediction of the variability of the solar irradiance GHI, under the influence of a frontal system in the desert region of northwestern Mexico. It was also possible to observe the importance of associating humidity characteristics to frontal systems as a potential factor that hindered model predictions in this study area. This analysis provides a configuration of the WRF model that can be used as a meteorological prediction tool to directly associate the variability of solar irradiation in the estimation of short-term electric power generation in solar-activated plants, under the influence of winter systems in desert regions. It is proposed in future work that the opt2 configuration be tested under different planetary boundary layer parameterization options, where its performance will be evaluated in other similar climatic regions, and the sample of frontal events with humidity characteristics associated with tropical maritime air masses be increased.

Author Contributions: Conceptualization, J.E.L.-V. and N.V.-L.; methodology, J.E.L.-V.; software, J.E.L.-V. and D.E.F.-J.; validation, J.E.L.-V., D.E.F.-J. and S.I.-P.; investigation, J.E.L.-V. and N.V.-L.; resources, N.S.-S.; data curation, J.E.L.-V., J.R.-A. and S.I.-P.; writing—original draft preparation, J.E.L.-V.; writing—review and editing, N.V.-L., S.I.-P. and D.E.F.-J.; visualization, J.E.L.-V. and S.I.-P.; supervision, N.V.-L. and N.S.-S.; project administration, N.V.-L. and N.S.-S. All authors have read and agreed to the published version of the manuscript.

Funding: This research received no external funding.

Institutional Review Board Statement: Not applicable.

Informed Consent Statement: Not applicable.

Data Availability Statement: Data available on request due to restrictions privacy.

Acknowledgments: The authors are grateful to the Engineering Institute of the Autonomous University of Baja California for the support given to carry out this project. To the National Council of Science and Technology (CONAHCYT) for the grant given to José Ernesto López Velázquez (559433). The authors acknowledge the Autonomous University of Baja California for the support received from (111/6/C/19/23) within the framework of the call "23a. Convocatoria Interna".

Conflicts of Interest: The authors declare no conflict of interest.

References

1. Pedro, H.T.C.; Coimbra, C.F.M. Assessment of forecasting techniques for solar power production with no exogenous inputs. *Sol. Energy* **2012**, *86*, 2017–2028. [CrossRef]
2. Diagne, M.; David, M.; Boland, J.; Schmutz, N.; Lauret, P. Post-processing of solar irradiance forecasts from WRF model at Reunion Island. *Sol. Energy* **2014**, *105*, 99–108. [CrossRef]
3. Neves, D.; Brito, M.C.; Silva, C.A. Impact of solar and wind forecast uncertainties on demand response of isolated microgrids. *Renew. Energy* **2016**, *87*, 1003–1015. [CrossRef]
4. Zempila, M.-M.; Giannaros, T.M.; Bais, A.; Melas, D.; Kazantzidis, A. Evaluation of WRF shortwave radiation parameterizations in predicting Global Horizontal Irradiance in Greece. *Renew. Energy* **2016**, *86*, 831–840. [CrossRef]
5. Incecik, S.; Sakarya, S.; Tilev, S.; Kahraman, A.; Caliskan, E.; Topcu, S.; Kahya, C.; Odman, M.T. Evaluation of WRF parameterizations for global horizontal irradiation forecasts: A study for Turkey. *Atmosfera* **2019**, *32*, 143–158. [CrossRef]
6. Hayat, M.B.; Ali, D.; Monyake, K.C.; Alagha, L.; Ahmed, N. Solar energy—A look into power generation, challenges, and a solar-powered future. *Int. J. Energy Res.* **2019**, *43*, 1049–1067. [CrossRef]
7. Enríquez-Velásquez, E.A.; Benitez, V.H.; Obukhov, S.G.; Félix-Herrán, L.C.; Lozoya-Santos, J.D.J. Estimation of Solar Resource Based on Meteorological and Geographical Data: Sonora State in Northwestern Territory of Mexico as Case Study. *Energies* **2020**, *13*, 6501. [CrossRef]
8. Dubey, A. Preparing the Power Grid for Extreme Weather Events: Resilience Modeling and Optimization. In *Women in Power: Research and Development Advances in Electric Power Systems*; Tietjen, J.S., Ilic, M.D., Bertling Tjernberg, L., Schulz, N.N., Eds.; Springer International Publishing: Cham, Switzerland, 2023; pp. 209–243. [CrossRef]
9. Añel, J.A.; Fernández-González, M.; Labandeira, X.; López-Otero, X.; la Torre, L. Impact of Cold Waves and Heat Waves on the Energy Production Sector. *Atmosphere* **2017**, *8*, 209. [CrossRef]
10. Busby, J.W.; Baker, K.; Bazilian, M.D.; Gilbert, A.Q.; Grubert, E.; Rai, V.; Rhodes, J.D.; Shidore, S.; Smith, C.A.; Webber, M.E. Cascading risks: Understanding the 2021 winter blackout in Texas. *Energy Res. Soc. Sci.* **2021**, *77*, 102106. [CrossRef]
11. Smith, A.B. 2022 U.S. Billion-Dollar Weather and Climate Disasters in Historical Context. Available online: https://www.climate.gov/news-features/blogs/beyond-data/2022-us-billion-dollar-weather-and-climate-disasters-historical (accessed on 7 May 2024).
12. National Oceanic and Atmospheric Administration. National Centers for Environmental Prediction, Weather Prediction Center. Available online: https://www.wpc.ncep.noaa.gov/dailywxmap/index.html (accessed on 14 June 2024).
13. West, S.R.; Rowe, D.; Sayeef, S.; Berry, A. Short-term irradiance forecasting using skycams: Motivation and development. *Sol. Energy* **2014**, *110*, 188–207. [CrossRef]
14. Steyn, D.G.; Oke, T.R.; Hay, J.E.; Knox, J.L. On scales in meteorology and climatology. *Climatol. Bull.* **1981**, *39*, 1–8.
15. Brisch, J.; Kantz, H. Power law error growth in multi-hierarchical chaotic systems—A dynamical mechanism for finite prediction horizon. *New J. Phys.* **2019**, *21*, 93002. [CrossRef]
16. Balzarini, A.; Angelini, F.; Ferrero, L.; Moscatelli, M.; Perrone, M.G.; Pirovano, G.; Riva, G.M.; Sangiorgi, G.; Toppetti, A.M.; Gobbi, G.P.; et al. Sensitivity analysis of PBL schemes by comparing WRF model and experimental data. *Geosci. Model Dev. Discuss.* **2014**, *7*, 6133–6171. [CrossRef]
17. Lara-Fanego, V.; Ruiz-Arias, J.A.; Pozo-Vázquez, D.; Santos-Alamillos, F.J.; Tovar-Pescador, J. Evaluation of the WRF model solar irradiance forecasts in Andalusia (southern Spain). *Sol. Energy* **2012**, *86*, 2200–2217. [CrossRef]
18. Cohen, A.E.; Cavallo, S.M.; Coniglio, M.C.; Brooks, H.E. A Review of Planetary Boundary Layer Parameterization Schemes and Their Sensitivity in Simulating Southeastern U.S. Cold Season Severe Weather Environments. *Weather Forecast* **2015**, *30*, 591–612. [CrossRef]
19. Prasad, A.A.; Kay, M. Assessment of Simulated Solar Irradiance on Days of High Intermittency Using WRF-Solar. *Energies* **2020**, *13*, 385. [CrossRef]
20. Mierzwiak, M.; Kroszczyński, K.; Araszkiewicz, A. On Solar Radiation Prediction for the East–Central European Region. *Energies* **2022**, *15*, 3153. [CrossRef]
21. Urias, H.E.; Cueto, O.R.G.; Morales, G.B. Identification and classification of local climate zones in a semi-arid city of northwestern Mexico. *Vivienda Comunidades Sustentables* **2021**, *9*, 45–60. [CrossRef]
22. Lazaridis, M. Atmospheric Circulation. In *First Principles of Meteorology and Air Pollution*; Springer: Dordrecht, The Netherlands, 2011; pp. 119–149. [CrossRef]
23. Romero-Arteaga, A.; Ruiz de Alegría-Arzaburu, A.; Rivas, D.; Juarez, B. Nearshore current variations during the passage of cold fronts in NW Gulf of Mexico. *Cont. Shelf Res.* **2022**, *238*, 104697. [CrossRef]
24. NASA POWER Prediction of Worldwide Energy Resources. National Aeronautics and Space Administration. Available online: https://power.larc.nasa.gov (accessed on 14 June 2024).
25. National Centers for Environmental Prediction National Weather Service NOAA U.S. Department of Commerce. NCEP GDAS/FNL 0.25 Degree Global Tropospheric Analyses and Forecast Grids. Research Data Archive at the National Center for Atmospheric Research, Computational and Information Systems Laboratory, Boulder, CO, USA. 2015. Available online: https://rda.ucar.edu/datasets/dsd083003/ (accessed on 10 September 2023).
26. Kheyruri, Y.; Sharafati, A.; Ahmadi Lavin, J. Performance assessment of NASA POWER temperature product with different time scales in Iran. *Acta Geophys.* **2024**, *72*, 1175–1189. [CrossRef]

27. Rodrigues, G.C.; Braga, R.P. Evaluation of NASA POWER Reanalysis Products to Estimate Daily Weather Variables in a Hot Summer Mediterranean Climate. *Agronomy* **2021**, *11*, 1207. [CrossRef]
28. Sauter, B. *A Case Study of the Persistence of Weather Forecast Model Errors*; Army Research Laboratory: Adelphi, MD, USA, 2005.
29. Mittermaier, M.P. The Potential Impact of Using Persistence as a Reference Forecast on Perceived Forecast Skill. *Weather Forecast* **2008**, *23*, 1022–1031. [CrossRef]
30. Skamarock, W.C.; Klemp, J.B. A time-split nonhydrostatic atmospheric model for weather research and forecasting applications. *J. Comput. Phys.* **2008**, *227*, 3465–3485. [CrossRef]
31. García-Díez, M.; Fernández, J.; Fita, L.; Yagüe, C. Seasonal dependence of WRF model biases and sensitivity to PBL schemes over Europe. *Q. J. R. Meteorol. Soc.* **2013**, *139*, 501–514. [CrossRef]
32. Perez, R.; Lorenz, E.; Pelland, S.; Beauharnois, M.; Van Knowe, G.; Hemker, K., Jr.; Heinemann, D.; Remund, J.; Müller, S.C.; Traunmüller, W.; et al. Comparison of numerical weather prediction solar irradiance forecasts in the US, Canada and Europe. *Sol. Energy* **2013**, *94*, 305–326. [CrossRef]
33. Ruiz-Arias, J.A.; Dudhia, J.; Santos-Alamillos, F.J.; Pozo-Vázquez, D. Surface clear-sky shortwave radiative closure intercomparisons in the Weather Research and Forecasting model. *J. Geophys. Res. Atmos.* **2013**, *118*, 9901–9913. [CrossRef]
34. Iacono, M.J.; Delamere, J.S.; Mlawer, E.J.; Shephard, M.W.; Clough, S.A.; Collins, W.D. Radiative forcing by long-lived greenhouse gases: Calculations with the AER radiative transfer models. *J. Geophys. Res. Atmos.* **2008**, *113*. [CrossRef]
35. Clough, S.A.; Shephard, M.W.; Mlawer, E.J.; Delamere, J.S.; Iacono, M.J.; Cady-Pereira, K.; Boukabara, S.; Brown, P.D. Atmospheric radiative transfer modeling: A summary of the AER codes. *J. Quant. Spectrosc. Radiat. Transf.* **2005**, *91*, 233–244. [CrossRef]
36. Chou, M.-D.; Suarez, M.J. *A Solar Radiation Parameterization for Atmospheric Studies, NASA Tech. Rep. Series on Global Modeling and Data Assimilation, NASA/TM-1999-104606*; NASA Goddard Space Flight Center: Greenbelt, MD, USA, 1999; Volume 15.
37. Gu, Y.; Liou, K.N.; Ou, S.C.; Fovell, R. Cirrus cloud simulations using WRF with improved radiation parameterization and increased vertical resolution. *J. Geophys. Res. Atmos.* **2011**, *116*. [CrossRef]
38. Marquez, R.; Coimbra, C.F.M. Proposed metric for evaluation of solar forecasting models. *J. Sol. Energy Eng.* **2013**, *135*, 11016. [CrossRef]
39. Taylor, K.E. Summarizing multiple aspects of model performance in a single diagram. *J. Geophys. Res. Atmos.* **2001**, *106*, 7183–7192. [CrossRef]
40. Pasch, R.J. National Hurricane Center, Tropical Cyclone Report:Tropical Storm Odalys (EP-202020). April 2021. Available online: https://www.nhc.noaa.gov/data/tcr/EP202020_Odalys.pdf (accessed on 13 June 2023).